Study of interfaces in Co/Cu multilayers by low-angle anomalous x-ray diffraction

A. de Bernabé
Instituto de Ciencia de Materiales de Madrid, Consejo Superior de Investigaciones Científicas, 28049 Cantoblanco, Spain and European Synchrotron Radiation Facility, B.P. 220, 38043 Grenoble, France

M. J. Capitán
European Synchrotron Radiation Facility, B.P. 220, 38043 Grenoble, France

H. E. Fischer
Institut Max von Laue-Paul Langevin, B.P. 156, 38042 Grenoble, France

C. Prieto[a)]
Instituto de Ciencia de Materiales de Madrid, Consejo Superior de Investigaciones Científicas, 28049 Cantoblanco, Spain

(Received 19 February 1998; accepted for pubication 5 May 1998)

The innovative method of combining specular and off-specular low-angle x-ray diffraction, along with the anomalous scattering effect, has been used to characterize magnetron-sputtered Co/Cu multilayers. The anomalous dispersion of Co is employed to increase the electron density contrast between the cobalt and copper layer. The use of a simulation program has been proven to be a straightforward and reliable method to analyze x-ray low-angle diffraction patterns in such a nonperfectly ordered metallic multilayer system. This method has been successfully applied to data obtained from synchrotron experiments and the results compared with those performed using a standard laboratory diffractometer. The combination of both specular and off-specular scans has ensured the obtention of a single set of simulation parameters for the structure of the multilayer and its interfaces. In addition, the off-specular scans have permitted us to confirm, in a rather complex system, the validity of the distorted wave born approximation. The mesoscopic structure of this multilayered system has been accurately and self-consistently characterized. © *1998 American Institute of Physics.* [S0021-8979(98)00816-0]

I. INTRODUCTION

For the purpose of explaining the unusual properties exhibited by the different types of superlattices, such as metal/metal,[1,2] or semiconductor/semiconductor,[3,4] a precise structural characterization has been essential. The role played by interfaces seems to be very important, especially in the context of giant magnetoresistance (GMR),[5–8] where there is need of an accurate determination of interfacial structure.

Among the multiple techniques used to characterize the structure of multilayers (such as nuclear magnetic resonance, Rutherford backscattering spectroscopy, neutron and x-ray diffraction, and scanning electron microscopy or SEM) the most widespread is probably x-ray diffraction.[9–11] X-ray diffraction is a nondestructive technique and gives a global measure of the sample's structure (unlike SEM). At high angles, x-ray diffraction yields information about a system at a crystallographic scale: structure, strains and domain sizes, while at small angles it yields information related to the mesoscopic structure of the material. At low angle x-ray diffraction, two kinds of experiments can be performed: specular scans which provide information about the dimension perpendicular to the surface of the multilayer (ML) permitting thus the determination of the layer thicknesses and root-mean-square (rms) roughness of the substrate (σ), interfaces and overlayer.[12] Off-specular scans (ω rock or rocking curves, and 2θ rocks or detector scans) allow the reconstruction of the height–height correlation function of the roughness.[13–16]

There are two fundamental ways of obtaining the information from the reflectivity patterns. One of them is the use of the Fourier analysis of data based on the Born approximation. This method permits us to obtain the autocorrelation function of the derivative of the sample's electron density profile. It has been proven to be quite useful in some cases,[17,18] however it must be used very cautiously and in some cases the results may not be easy to interpret. When the system to be characterized is almost perfect (high degree of crystallinity and sharp interfaces as in semiconductor superlattices), the pattern obtained after the Fourier transform will be quite clear. However for thick metallic superlattices a great variety of growth defects may appear (such as high roughnesses or variations in the layer thicknesses). In this case, the Fourier analysis does not give much information on the sample's structure.

Alternatively, one can simulate reflectivity curves using a matricial calculation.[12,19–21] Through this method, an accurate and self-consistent structural determination can be achieved when specular scans are completed by off-specular

[a)]Electronic mail: cprieto@icmm.csic.es

scans (ω rock and 2θ rock curves), which probe the in-plane structure of the ML and not simply the average electron density profile [$\rho(z)$] probed by specular scans.

Our aim in the present paper is threefold: first, we want to emphasize the need for using the anomalous dispersion techniques for systems in which the electron density contrast is very low. Only by using the anomalous (resonant) dispersion effect can a pattern with sufficient contrast and extent within the wave vector ($\mathbf{q}$) region be obtained; second, the fit of the experimental results with a computer simulation program is the method that gives the most complete and reliable characterization of the system; and finally, the combination of specular and off-specular experiments results in the obtention of a single set of self-consistent parameters which describe the system. This all has been proven in a set of Co/Cu multilayers in which the mesoscopic structure has been completely characterized.

II. EXPERIMENT

Samples were grown on a Si (100) oxidized substrate using a dc-operated magnetron sputtering system with a residual pressure of 5×10^{-7} mbar. The Ar pressure used for deposition was 4.8×10^{-3} mbar at a constant substrate temperature of 60 °C. The substrate was placed 8 cm away from magnetrons in order to get a good in-plane homogeneity of the sample. The deposition rates obtained were 2 nm/min for Co and 3 nm/min for Cu. Specially designed stainless steel screens were used to avoid mixing of Co and Cu during growth. The total sample thickness for the whole set was kept nearly constant around a value of 70 nm, for which the number of bilayers was varied; no buffer was used for growth. The samples grown with a Co/Cu thickness ratio equal to unity are represented as $[m\mathrm{Cu}/m\mathrm{Co}]_n$, where m is the layer thickness in Å and n the number of layers. The samples presented in this paper are: $(50\ \mathrm{Cu}/50\ \mathrm{Co})_7$, $(33\ \mathrm{Cu}/33\ \mathrm{Co})_{10}$, $(24\ \mathrm{Cu}/24\ \mathrm{Co})_{13}$, $(19\ \mathrm{Cu}/19\ \mathrm{Co})_{17}$, $(17\ \mathrm{Cu}/17\ \mathrm{Co})_{20}$ and $(9\ \mathrm{Cu}/9\ \mathrm{Co})_{40}$.

The early x-ray specular-reflectivity measurements were performed on a standard Siemens D-500 two-circle diffractometer. The wavelength used was the K_α radiation line of Cu ($\lambda=1.54$ Å) with a graphite analyzer before the detector to avoid the $K_{\alpha2}$ radiation line of copper. Incident and collection slits were chosen to be 0.3°, which gave the best product signal resolution. The Cu target was operated at 40 keV and with a tube current of 25 mA. The dynamic range of the detector could not allow the recording of the entire reflectivity patterns, as a consequence of which reflectivity patterns from the standard diffractometer were saturated at very low angles.

X-ray resonant low-angle diffraction experiments were carried out on the four circle goniometer setup at D23 beamline (LURE-DCI, Orsay, France).[22] The beamline is equipped with a double crystal [Si(111)] monochromator with fixed exit and sagittal focusing. The experiments were performed 5 eV under the Co absorption K edge, which was determined previously by recording the near edge x-ray absorption structure spectrum, to obtain the edge precisely. The detection was done combining an avalanche photodiode[23] with a Ge(111) crystal analyzer tuned at the incident beam wavelength. The use of the analyzer permits us to increase the angular resolution and the signal to background ratio by suppressing fluorescence. On the other hand, the avalanche photodiode has a good dynamic range (up to 50 000 counts/s). The instabilities of the incident beam were monitored through the diffuse scattering from a kapton film, recorded and corrected automatically in the data acquisition program. The experimental resolution function (a convolution of the slits used, beam divergence and the resolution of the detector) obtained from a rocking curve was 40 arcsec with an incident beam dimensions of 0.1×6 mm. A set of secondary slits placed just before the detector was set to 200 μm so as to get rid of diffuse scattering queues present in the ω scans.

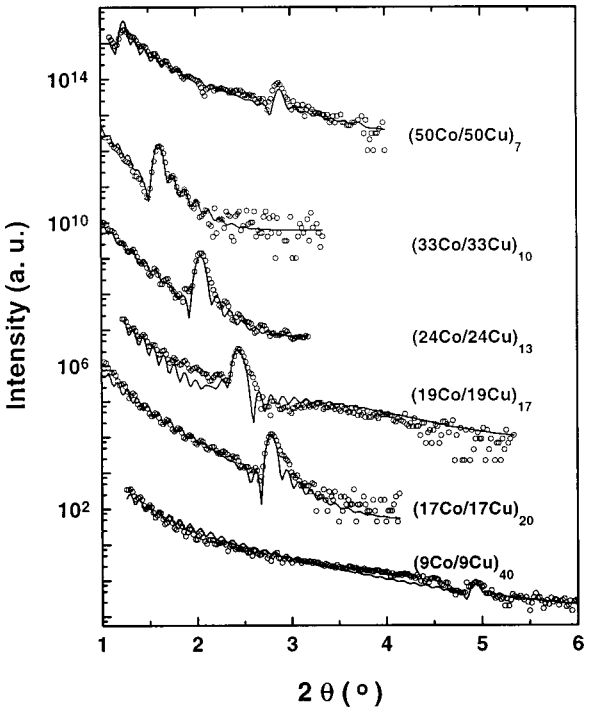

FIG. 1. Specular reflectivity patterns of Co/Cu multilayers recorded at an incident energy of 8052 eV. Points correspond to the experimental patterns and solid lines have been calculated by the described simulation program.

Using the standard D-500 diffractometer only specular scans were performed. While using synchrotron radiation at energies near the Co edge three kind of experiments were done: specular scans (ω-θ); rocking curves or ω rocks (taken at a constant 2θ) and 2θ rocks (in which ω is constant). For the rocking curves, the detector was placed at an angle 2θ coinciding with a secondary maximum (Kiessig fringe) at around 1.3°. They were chosen to be on a secondary maximum near the critical angle to obtain the highest contrast and good detail.

III. EXPERIMENTAL DATA

Figures 1 and 2 show the experimental reflectivity patterns obtained using a standard diffractometer (with an incident energy of 8052 eV) and synchrotron radiation (in order to make use of the Co anomalous dispersion the incident energy was 7704 eV). In both of them, the hollow points

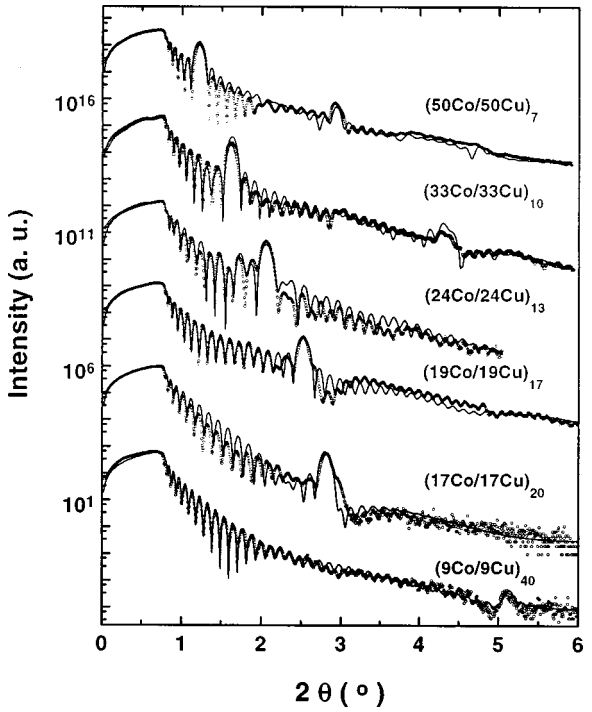

FIG. 2. Specular reflectivity patterns of Co/Cu multilayers recorded at an incident energy just under the Co absorption *K* edge (7704 eV). Points correspond to the experimental patterns and solid lines have been calculated by the simulation program.

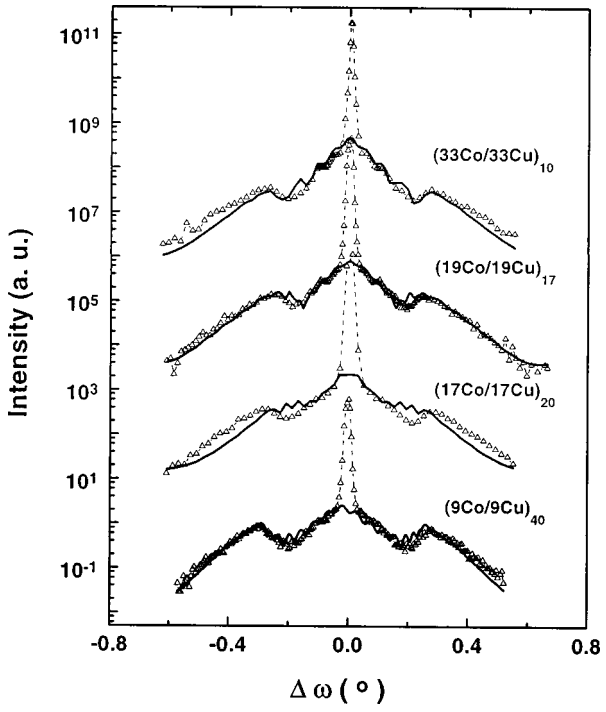

FIG. 3. Rocking curves taken at constant values of 2θ placed at a Kiessig maximum around $2\theta_M = 1.32°$. For the sake of clarity $\Delta\omega = \omega - \theta_M$ has been taken as the variable. The fits to the experimental patterns are based on the DWBA. The specular peak has not been reproduced in the simulations.

represent the experimental data, and lines are the mean square fits using the below described simulation program. Patterns correspond to six different samples with bilayer thicknesses ranging from 18 to 100 Å, in which the intensity position has been shifted in order to plot all the patterns together. Let us note that while in Fig. 2 patterns start at an angle $2\theta = 0°$, in Fig. 1 they are plotted from $2\theta = 1°$. The reason for that is nothing but the saturation of the standard diffractometer detector, which did not allow to go to lower angles.

The small oscillations present in the spectra correspond to sample-size oscillations (usually called Kiessig fringes). They arise from multiple interference between beams reflected at the top interface and at the multilayer–substrate interface. Superimposed to the Kiessig fringes, the multilayer peaks appear (they are Bragg-like peaks coming from the chemical modulation of the sample) which account for the periodicity of the ML. The number of Kiessig fringes between each pair of Bragg peaks is $2n-1$, '' n'' being the number of deposited bilayers. An inspection of these fringes permits us to check that the number of bilayers used in the simulation is correct. Finally, some long wavelength oscillation can be observed in some samples, which can be attributed to a thin oxide overlayer.

Figure 3 shows the rocking curves corresponding to four samples. They have been taken at somehow different values of 2θ in order to be placed at a secondary (Kiessig) maximum in all of them and have an optimal contrast. They have been taken near the total reflection angle in order to see the dynamic effects in the MLs. Such effects are seen, in addition to the small oscillations near the central peak, through the so-called Yoneda wings[24] (which are broad maxima at both extrema of the plots after which the intensity drops sharply). They arise from interferences of the diffuse scattering by different interfaces and they are not reproducible within the Born approximation. The spectrum (17 Co/17 Cu)$_{20}$ may be the most inaccurate probably due to a lower quality of the ML (something which matches well with the specular pattern), while the spectrum corresponding to (19 Co/19 Cu)$_{17}$ manages to reproduce perfectly the structure and the Yoneda wings.

The last type of scans are the 2θ rocks. They are done at a constant value of ω, which is half of the value of 2θ at which the rocking curves were taken. This scan geometry permits us to see the reciprocal space in both the x and z directions. Figure 4 shows the spectra corresponding to the four samples from which ω rocks were taken. In the spectrum corresponding to the (33 Co/33 Cu)$_{10}$ sample there is an important increase in the oscillation at $2\theta = 1.6°$. This comes from an intensity leakage of the first Bragg peak of the multilayer, as can be seen from a glance at Fig. 4. In all the scans, the amplitude of the oscillations (related to vertical correlation length) as well as the intensity tendency (coming from the horizontal correlation length) are well reproduced, allowing us to rely on the values of the correlation lengths.

IV. DATA ANALYSIS AND DISCUSSION

A. Anomalous diffraction

As it can be observed from a direct comparison between Figs. 1 and 2, there is a remarkable difference in their patterns arising from the change in the electron density contrast

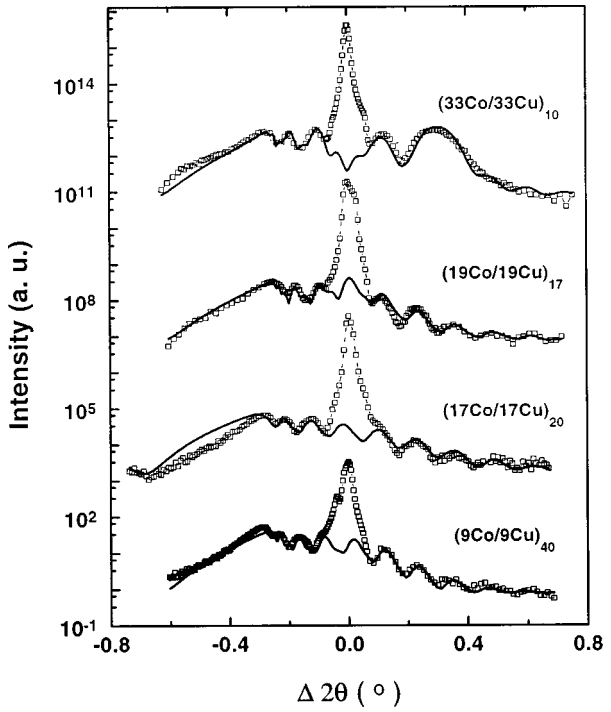

FIG. 4. 2θ rock curves with their fit. The value of ω was held constant and around 0.66°. The variable used is $\Delta 2\theta = 2\theta - 2\theta_M$. For the simulations only the diffuse intensity has been taken into account.

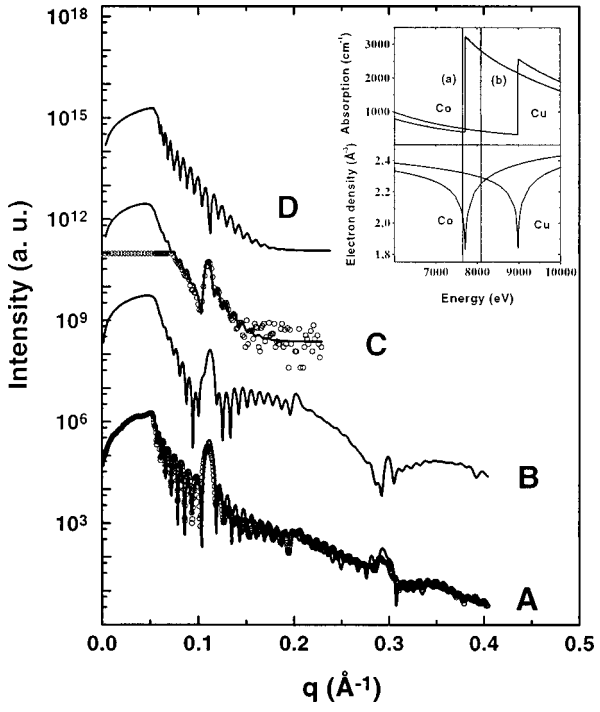

FIG. 5. Experimental and calculated reflectivity spectra for the (33 Co/33 $Cu)_{10}$ sample. Spectra *A* and *C* are the experimental patterns taken at 7704 and 8052 eV, respectively (fits have been plotted by using a continuous line). The *B* curve is a simulation with the same parameters obtained from the *A* spectrum fit, but for an energy of 8052 eV. The *D* curve is a simulation with the same parameters obtained from the *C* spectrum fit except that the Co and Cu absorption values have been taken equal for both of them (contrary to the situation at 8052 eV where the *C* spectrum was performed). The inset shows the absorption coefficients and the electron densities for Co and Cu. Vertical lines have been plotted at the energies at which the experiments were performed.

between Co and Cu at the two incident energies used. To see it more clearly, we present next the scattering cross section of a rough interface, which was calculated for the first time using the distorted wave Born approximation (DWBA) by Sinha *et al.*[13] and later extended by Holý and Baumbach[14,15] to layered systems. For a surface between two media with an electron density contrast of $\Delta\rho$, the scattering cross section is given by:[13]

$$S(q) = |T(\alpha)|^2 |T(\beta)|^2 \frac{A\Delta\rho^2}{|q_z^2|} e^{-\frac{1}{2}\sigma^2(\overline{q_z^2}+\overline{q_z^{*2}})} \times \int\int dx\, dy\, e^{|\overline{q_z}|^2 C(R)} e^{-i(q_x x + q_y y)}, \quad (1)$$

where $T(\alpha)$ $[T(\beta)]$ is the transmission coefficient of that interface for the grazing angle of incidence (collection); *A* is the illuminated area; **q** is the scattering wave vector; σ is the rootmean-square roughness of the surface and $C(\mathbf{R})$ is the height–height correlation function (**R** is the lateral position), which describes the morphology of the surface.[25] For a multilayer, the total scattered intensity must account for the intensity scattered at each interface of the ML, which will depend on the electron density contrast between the elements forming the ML. The consequence of this result is that the intensity of the Bragg peaks arising from the additional periodicity of a multilayer is proportional to the square of the refraction index contrast between its elements. As the inset in Fig. 5 shows, at the energy of Cu K_α radiation, $E=8052$ eV, the electron density contrast between the Co and the Cu is almost zero, while there exists a high difference in their absorption coefficients. On the contrary, just under the Co absorption edge, $E=7704$ eV, the contrast is given by the difference in the electron density. In fact, at 8052 eV, the Bragg peak comes just from the absorption difference between Cu and Co. To see it more clearly and in order to compare the advantages of using the anomalous scattering of atoms, four spectra have been plotted in Fig. 5. In this figure spectra *A* and *C* show the experimental patterns with their fits for (33 Co/33 $Cu)_{10}$ sample using synchrotron radiation at 7704 eV (for the *A* spectrum) and using the standard diffractometer at an incident energy of 8052 eV (for the *C* spectrum), where the electron density contrast is lower. Let us note that in the *C* spectrum, we have extended the wave vector region to $\mathbf{q}=0$ in order to get a clearer comparison. The difference between both spectra is evident: in the *A* spectrum the Bragg peaks can be observed up to the third order and the Kiessig fringes are perfectly seen over all the spectrum; on the other hand, in the *C* spectrum only one multilayer peak can be observed, with a lower contrast (in the Kiessig fringes too) and only background noise is seen from $\mathbf{q}\sim 0.15 Å^{-1}$. Along with these two plots, the *B* spectrum permits us to see the differences in the reflectivity pattern coming from the advantage of the anomalous dispersion or from the use of a different characterization source (synchrotron radiation versus standard diffractometer). Looking at the *B* spectrum, one may think that a third order Bragg peak may also be seen; however the intensity decreases two orders of magnitude from $\mathbf{q}=0.2$ $Å^{-1}$ and a contrast even

higher than that obtained would be needed to distinguish the peaks from the background. As it can be in the inset, at 8052 eV the Co and Cu electron densities are practically equal (vertical line marked as E_b), therefore the Bragg peaks observed in the *C* curve come just from the difference in their absorption coefficients. To see this better, the *D* spectrum has been plotted. It is a simulation which has been calculated with exactly the same parameters obtained in the fit of the *C* one but equal to the absorption of Co and Cu ($\mu_{Cu}=\mu_{Co}=385\ cm^{-1}$). As it can be seen, the Bragg peak has totally disappeared and the only remaining feature is a slight decrease of the intensity just at the former peak angle. Fig. 5 proves how the anomalous dispersion permits us to obtain higher quality results which help us to determine more accurately the structural parameters of the ML.

B. Fourier transform

As explained in Sec. I, one way to analyze x-ray reflectivity patterns is to perform the Fourier transform (FT) of the experimental results. This analysis is based on the fact pointed out in the literature[17] that the reflectivity can be approximately expressed, for wave vectors larger than the critical, as:

$$R(q)\propto \frac{\left|\int_{-\infty}^{\infty}\frac{dn}{dz}e^{iqz}dz\right|^2}{q^4}, \tag{2}$$

where **q** is the scattering wave vector and *n* the refractive index. The autocorrelation function (ACF) of the derivative of the density profile $[\rho(z)]$, defined as:

$$\rho(z)=\int_{-\infty}^{\infty}\frac{\partial n}{\partial z}(t)\frac{\partial n}{\partial z}(t-z)dt \tag{3}$$

can be written, taking into account its definition and Eq. (2), as

$$\rho(z)\propto\int_{-\infty}^{\infty}q^4R(q)e^{iqz}dq, \tag{4}$$

which is just the FT of the reflectivity pattern multiplied by the wave vector **q** to the fourth power. When the multilayer has perfect interfaces, the ACF is a Dirac delta, but when there is roughness, the Dirac function turns into a Gaussian distribution (which is nothing but the FT of the derivative of an error function).

Even it the FT of the reflectivity profile is a quite simple method; when the superlattice deviates from an ideal case, the obtained results as well as the interpretation are not trivial. To illustrate this assertion, we have performed several simulations for a $(33\ Cu/33\ Co)_{10}$ multilayer with different roughnesses, increasing from no roughness ($\sigma=0$) to $\sigma=8$ Å. We have then applied the FT as in Eq. (4) to the simulations. The obtained results are presented in Fig. 6. In the lowest graph ($\sigma=0$), the peaks corresponding to each interface are perfectly reproduced (indeed, as explained previously, they should correspond to Dirac functions, something which does not happen because of the process used to perform the FT, which is also responsible for the ''side loves'' appearing at the bottom of the peaks). These peaks appear at depths corresponding to multiples of the single layer thickness (around 33 Å). In addition, a broad and intense peak appears at around 660 Å, arising from the first layer–substrate interface. As the roughness is increased, the oscillations are reduced. At about $\sigma=8$ Å, no information about the layer thicknesses can be extracted from the pattern. Furthermore, if in addition to the roughness there are other kind of inhomogeneities in the sample, such as fluctuations in the layer thicknesses, the patterns become quite difficult to interpret.

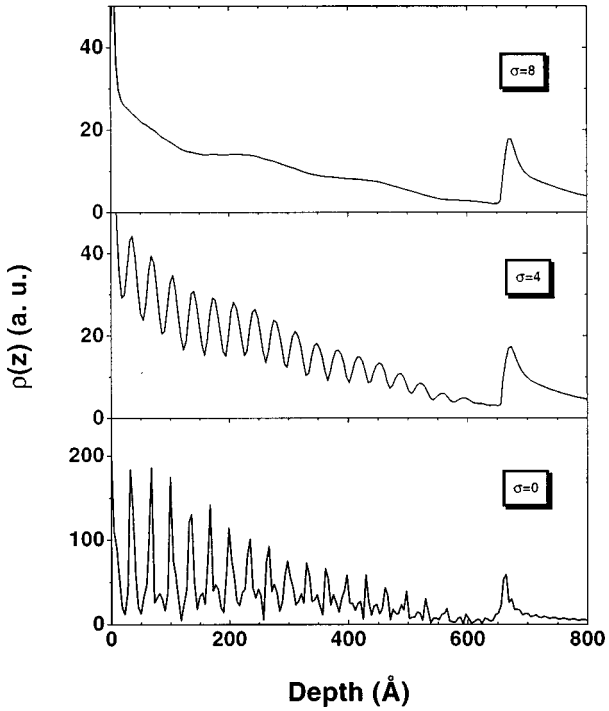

FIG. 6. Fourier transform as indicated in Eq. (4) where $R(q)$ has been obtained by simulation of a $[33\ Cu/33\ Co]_{10}$ multilayer with three different interface roughnesses.

We have then followed this method to have a preliminary overall picture of our multilayers. In Fig. 7 we have represented four FT patterns corresponding to two samples. The numbers in each plot refer to the corresponding peak position. *A* and *B* plots correspond to sample $(50\ Co/50\ Cu)_7$ but at the two incident energies used, 7704 and 8052 eV, respectively. Both yield interface positions very similar to one another, yet have the former higher contrast and extent of the oscillations. The values corresponding to the first peaks in the FT are given within the plot and match quite well the expected results (50 Å for each layer thickness). *C* and *D* plots correspond to the sample $(33\ Co/33\ Cu)_{10}$, at 7704 and 8052 eV, respectively. Even if the peak positions in the *C* plot correspond approximately to the expected interfaces (an estimation from the Bragg peak positions yield 66 Å for the bilayer thickness), the contrast is very low, indicating that the roughness is high and the homogeneity of the layer thickness is not perfect. On the other hand, the *D* plot does not reproduce the ML modulation wavelength. This is understood since in the reflectivity pattern there is only one ML peak, making this method unuseful. The rest of the samples present a similar behavior under the FT yielding no useful information.

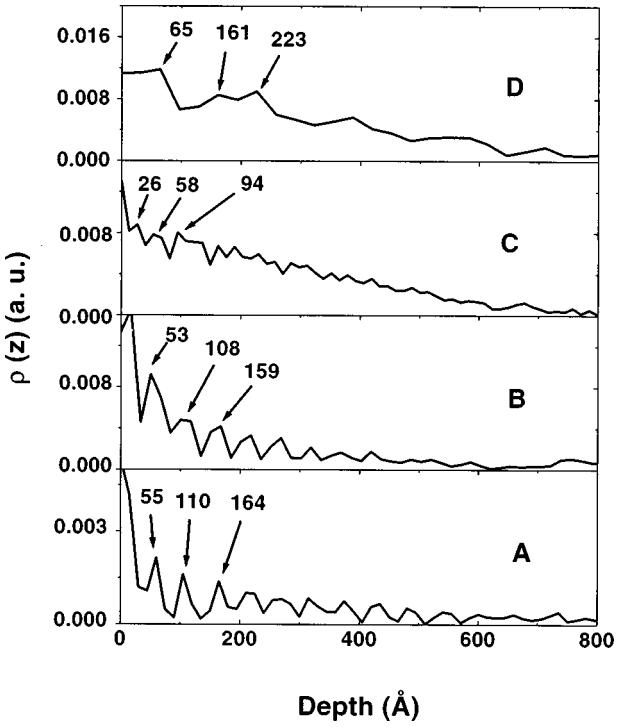

FIG. 7. Fourier transform as indicated in Eq. (4) of the experimental reflectivity. (a) Data obtained for $(50\ \mathrm{Co}/50\ \mathrm{Cu})_7$ at incident energy of 7704 eV. (b) The same sample at 8052 eV. (c) Data obtained for $(33\ \mathrm{Co}/33\ \mathrm{Cu})_{10}$ at incident energy of 7704 eV. (d) The same sample at 8052 eV.

This reinforces the following ideas: first, the need for using anomalous diffraction to obtain more multilayer Bragg peaks and higher contrast in the reflectivity patterns; second, the use of a simulation program to obtain the information becomes necessary to obtain complete information of the system or even just when its complexity is rather high.

C. Simulation methods

In order to obtain a quantitative and precise characterization of samples, obtained patterns have been fitted using the following simulation program (a detailed description will be reported elsewhere[26]). For specular scans, the formalism given by Vidal and Vincent[19] has been used and the patterns have been fitted by a least square procedure. The DWBA presented by Daillant and Bélorgey[27] has been used for the off-specular simulations. The computer program permits us to take into account a great number of parameters which influence the reflectivity pattern obtained: layer thicknesses, roughnesses, deviations from ideal cases (a linear and a Gaussian variation of the layer thicknesses, a linear stretch of the roughnesses,...), as well as the roughness correlation lengths ξ_x and ξ_z and parameter h, explained later in the section.

The electron densities and the absorption coefficients of the substrate, Co, Cu and the oxide layer, have been taken from the Sasaki tables.[28] They have been used as input parameters and then refined with the simulation program. Special attention has been paid to the Co and its oxide electron density for two reasons: first, close to the absorption edge the values for the Co scattering factor differ slightly among the different tables (Sasaki, Henke,...); second, the Co oxide produced at the surface may be of various kinds. In our fits, the electron density calculated for Co ($\rho_e^{\mathrm{Co}}=1.737\ \mathrm{Å}^{-3}$ at $E=7704$ eV) gives a critical angle that matches quite well the experimental one. For the oxide layer a compound Co_3O_4 seems to be the most frequent and stable for thin films at ambient temperature,[29] while in bulk form it is CoO the usual stoichiometry. Calculations of their electron density yield 1.36 and 1.40 $\mathrm{Å}^{-3}$ for Co_3O_4 and CoO, at the incident energy of $E=7704$ eV, respectively. An input parameter for the electron density of the oxide layer of 1.3 $\mathrm{Å}^{-3}$ has been used and the value fitted by a least square procedure. The obtained result, slightly under 1.40 $\mathrm{Å}^{-3}$, lies between the expected electron densities of both oxides, suggesting that the possibility of existence of both oxides cannot be neglected.

The fitting procedure was the next: once the parameters had been obtained from the specular patterns, they were used to simulate the off-specular scans in which only ξ_x, ξ_z, h and the roughnesses were varied. If no good fit could be obtained, the new roughness values were introduced into the reflectivity simulations and varied to obtain a better fit. Again, those parameters were used to do the off-specular simulations and the processes repeated until a single set of roughness parameters was obtained. This process was performed only in the four samples having both specular and off-specular scans. In the off-specular scans, the ξ_x obtained in the ω rocks was used to simulate the 2θ rocks and ξ_z was then varied until a good fit was reached.

To obtain the error bars, once the optimal fit had been reached by a rms process, the fit parameters were varied manually. When an appreciable change between the calculated and the experimental patterns had been observed, the difference was taken as the error bar.

Some special features should be taken into account to fit a particular sample, for instance $(33\ \mathrm{Co}/33\ \mathrm{Cu})_{10}$ sample in Fig. 2, the fact that the second order at about 3° is seen (while even orders should not be seen since the Co and Cu thicknesses are equal) and that the third one at 4.5° is so weak and double, means that there is a deviation from the ideal case. For the fit a Gaussian distribution of the layer thickness centered at Λ (bilayer thickness) 33 Å and with a full width at half maximum equal to 0.2 Å has been used.

For other samples a linear stretch of the roughness or a thickness gradient should be taken into account. In $(17\ \mathrm{Co}/17\ \mathrm{Cu})_{20}$ after the ML peak, the Kiessig oscillations cannot be seen anymore. The broadening undergone by the Bragg peak points toward a slight variation in the layer thicknesses. In the simulation, a linear thickness gradient of 0.2%/mm has been included, which improved the fit considerably. This linear variation of the layer thicknesses during growth can be understood as a monotonously continuous change of growing conditions. Finally, in $(9\ \mathrm{Co}/9\ \mathrm{Cu})_{40}$ a linear stretch of the Cu and Co roughnesses ($[\sigma_N-\sigma_0]/\sigma_0$) has been used in the fit, yielding 16% for Co and 13% for Cu ($\Lambda=18$ Å).

Even if the specular reflectivity patterns provide very good and precise structural parameters of the system when dealing with roughness, more than one possible solution may be obtained if diffuse scattering data were not accounted for.

TABLE I. Values obtained by the least square fit at two different energies: at 8052 eV, with a standard diffractometer, and at 7704 eV, using synchrotron radiation.

	Thickness of Co layer d_{Co} (Å)	Thickness of Cu layer d_{Cu} (Å)	Co rms roughness σ_{Co} (Å)	Cu rms roughness σ_{Cu} (Å)	Oxide layer thickness d_O (Å)	Oxide layer roughness σ_O (Å)	Substrate roughness σ_s (Å)	Horizontal correlation length ξ_x (Å)	Vertical correlation length ξ_z (Å)	Hurst parameter h
*(9 Co/9 Cu)$_{40}$[a]	9.0	9.0	7	7	3	2.0	11	⋯	⋯	⋯
(8052 eV)	±0.3	±0.3	±1	±1	±2	±0.5	±2			
(9 Co/9 Cu)$_{40}$	9.1	9.1	9	9	13	13.	13	6000	700	0.45
(7704 eV)	±0.1	±0.1	±1	±1	±1	±0.5	±2	±500	±200	
*(17 Co/17 Cu)$_{20}$[a]	15.6	17.6	11	7	8	7.0	13	⋯	⋯	⋯
(8052 eV)	±0.5	±0.5	±1	±1	±2	±0.7	±2			
(17 Co/17 Cu)$_{20}$	17.1	17.0	12	12	18	8.0	12	5000	650	0.45
(7704 eV)	±0.2	±0.2	±1	±1	±2	±0.5	±2	±2000	±100	
*(19 Co/19 Cu)$_{17}$[a]	19.7	18.3	8	8	21	4.5	12	⋯	⋯	⋯
(8052 eV)	±0.4	±0.4	±1	±1	±4	±0.3	±2			
(19 Co/19 Cu)$_{17}$	19.1	19.1	8	8	50	3.0	8	8000	900	0.4
(7704 eV)	±0.2	±0.2	±1	±1	±2	±0.2	±2	±2000	±100	
*(24 Co/24 Cu)$_{13}$[a]	26.6	20.6	11	13	7	11	15	⋯	⋯	⋯
(8052 eV)	±0.4	±0.5	±1	±1	±2	±3	±2			
*(24 Co/24 Cu)$_{13}$	23.5	23.5	9	9	23	5	8	⋯	⋯	⋯
(7704 eV)	±0.2	±0.2	±1	±1	±2	±1	±2			
*(33 Co/33 Cu)$_{10}$[a]	32.2	32.2	12	12	6	12	17	⋯	⋯	⋯
(8052 eV)	±0.5	±0.5	±1	±1	±2	±1	±2			
(33 Co/33 Cu)$_{10}$	33.0	33.0	12	6	33	4.5	10	8500	700	0.5
(7704 eV)	±0.3	±0.3	±2	±2	±1	±0.5	±2	±500	±50	
*(50 Co/50 Cu)$_7$[a]	46.3	49.7	6	6	8	4	14	⋯	⋯	⋯
(8052 eV)	±0.4	±0.4	±1	±1	±1	±2	±2			
*(50 Co/50 Cu)$_7$[a]	49.8	49.8	7	6	45	2.5	14	⋯	⋯	⋯
(7704 eV)	±0.2	±0.2	±1	±1	±5	±0.5	±1			

[a]Samples having an asterisk mean that only the specular scans have been used to obtain their parameters. From left to right, given values are: thickness of the Co layer, thickness of the Cu layer, Co rms roughness, Cu rms roughness, oxide layer thickness, oxide layer roughness, substrate roughness, horizontal correlation length, vertical correlation length and Hurst parameter.

This observation, already stated in the literature[16], led us to perform off-specular scans in our samples to obtain a single solution to the roughnesses. In addition, they have permitted us to obtain the correlation lengths of the roughness profiles as well as the Hurst parameter, the combination of which permits us to describe the morphology of the multilayer interfaces. The horizontal correlation length (ξ_x), represents approximately the distance between horizontal bumps. It allows us to determine if there exists interdiffusion ($\xi_x < 15$ Å) or interface roughness ($\xi_x > 15$ Å). On the other hand, the vertical correlation length (ξ_z) gives an idea of the vertical distance throughout which the interfaces can be correlated. The Hurst parameter (h) ranges from 0 to 1 and gives an idea of the kind of interface. A value near zero will be characteristic of a jagged interface while a value near one is typical of flat and wide bumps in the interface.

For the rocking curve simulations of Fig. 3, the diffuse intensity has been taken into account. That is the reason why the central peak is not reproduced. Typically, the rocking curves are very well reproduced by the simulation as in the (9 Co/9 Cu)$_{40}$ sample, except for the structure peaks which are not resolved in the background (due to a weak contrast). In the sample (33 Co/33 Cu)$_{10}$, the oscillations due to the structure are perfectly reproduced (except near the Yoneda wings). Nevertheless, the intensity fall after the critical angle would be reproduced better with a lower Hurst exponent ($h < 0.5$), indicating that our interfaces are rather jagged. Since computing time diverges when the h parameter deviates from 0.5, we did not consider it worth going to lower h values.

Again only the diffuse scattering has been used to do the simulations. In three of the spectra [all but the (17 Co/17 Cu)$_{20}$] there is a certain mosaicity, which can be clearly seen in the central peak. This is evident in the case of (9 Co/9 Cu)$_{40}$, where a double central peak is present. All the simulations manage to reproduce very well the 2θ patterns except maybe after the critical angle. This is not surprising since the scans are taken at a grazing angle ω of about 0.7°, and at very low positions of the detector ($2\theta < 2\theta - \omega_C$), there may exist border effects due to a slight misalignment, sample boarder effects or even a beam position shift [let it be noted that the shoulder present in the 2θ scan of (33 Co/33 Cu)$_{10}$ just under the critical value is exactly the same appearing in its specular pattern].

The simulation results are summarized in Table I. This table contains the parameters obtained from both the spectra taken with the standard diffractometer and those coming from the synchrotron radiation source. Samples having an asterisk mean that only the specular scans have been used to obtain their parameters. In Table I, even if the layer thicknesses are quite well reproduced, there exists some difference concerning the roughness. It has to be pointed out as well that there is a difference existing between the oxide layer thicknesses obtained with the commercial diffractometer and using synchrotron radiation. The reason for this is

nothing more than the fact that experiments were done in different times and that samples had undergone a slight oxidation which affected only the uppermost layer.[30]

Let it note that the values obtained from the reflectivity patterns at the two incident energies differ more than the error bars. However, the sum of both individual thicknesses is almost exact and well within the estimated errors [except maybe the $(17\ \mathrm{Co}/17\ \mathrm{Cu})_{20}$ sample for which the shoulder on the right side of the Bragg-like peak as well as its width yielded a larger error and mismatch between the multilayer periods obtained at $E=7704$ and 8052 eV]. The problem here is obtaining the thicknesses of Co and Cu separately. This problem, already overcome at high angles[11] has not, to our knowledge, been solved for low-angle patterns yet. Attempts are currently being done to try to obtain both thicknesses separately with a high degree of accuracy.

In our $E=7704$ eV reflectivity patterns, nevertheless, there is clear evidence that the thicknesses of both Co and Cu are almost exact. It is a fact that the even orders of the Bragg-like peaks do not appear in these patterns [see for example, near $2\theta=3°$ for the $(33\ \mathrm{Co}/33\ \mathrm{Cu})_{10}$ sample, or around $2\theta=5°$ in the $(19\ \mathrm{Co}/19\ \mathrm{Cu})_{17}$ sample]. At $E=8052$ eV, however, the low contrast does not allow us to obtain several low-angle diffraction orders and thus the totally reliable parameter is the bilayer thickness. All these considerations support, once again, the advantage of using anomalus x-ray scattering.

At this point it seems worth mentioning the validity of the DWBA, which can reproduce perfectly the off-specular scans even near the critical angles. A quite remarkable work by Schlomka *et al.*[16] concerning this subject was done recently. They studied the specular and transverse diffuse scans of several samples with an increasing degree of complexity. The DWBA reproduced perfectly the off-specular scans of a Ge layer, then a Ge/Si bilayer and finally a three layer system: Ge/Si/Ge, taken at different wave vector transfer. In the present case, we are not dealing with a three layer epitaxial system, but with a more complicated ML. Our samples have between 10 and 20 bilayers, with increasing roughnesses, varying thicknesses and with thick oxide layers. Even so, the ω rocks manage to reproduce remarkably well the shape and position of the dynamic peaks. These results lead to the same conclusions as those from Schlomka and co-workers in their previous work, enabling us to support the validity of the DWBA as a very good approach for calculating the x-ray scattering cross section of rough interfaces near the critical angle.

V. CONCLUSIONS

Anomalous x-ray reflectivity has been used to study a set of magnetron-sputtered Co/Cu multilayers. The use of the anomalous scattering and synchrotron radiation has allowed us to obtain higher contrast and a wider scanned angular range, which have permitted us to determine accurately the structure parameters of the system. In addition, the two ways of obtaining information from an x-ray reflectivity pattern have been compared by using a simulation program more reliable and accurate than the FT method. Finally, the combination of specular and off-specular scans has ensured the obtention of a single set of parameters which may be taken as the actual solution to the system. The mesoscopic structure of the Co/Cu multilayers has been accurate and unambiguously determined.

ACKNOWLEDGMENTS

The authors gratefully acknowledge Dr. Lefebvre and Dr. Bessières from Line D23 at LURE for providing support for and during the experiments. One of us, A. de B., wishes acknowledge his stay at ESRF where he performed this work. This work has been partially supported by the CICyT under Contract No. MAT97/0725.

[1] M. N. Baibich, J. M. Broto, A. Fert, F. Nguyen Van Dau, F. Petroff, P. Eitienne, G. Creuzet, A. Friedrich, and J. Chazelas, Phys. Rev. Lett. **61**, 2472 (1988).
[2] S. S. Parkin, R. Bhadra, and K. P. Roche, Phys. Rev. Lett. **66**, 2152 (1991).
[3] P. Voisin, G. Bastard, C. E. T. Goncalves da Silva, M. Voos, L. L. Chang, and L. Esaki, Solid State Commun. **39**, 79 (1981).
[4] B. Abeles and T. Tiedje, Phys. Rev. Lett. **51**, 2003 (1983).
[5] E. E. Fullerton, D. M. Kelly, J. Guimpel, I. K. Schuller, and Y. Bruynseraede, Phys. Rev. Lett. **68**, 859 (1992).
[6] H. E. Fischer, F. Petroff, F. Beliën, S. Lequien, G. Verbank, Y. Bruinseraede, S. Lefebvre, and M. Bessière, J. Phys. III **4**, 121 (1994).
[7] M. Suzuki, Y. Taga, A. Goto, and H. Yasuoka, Phys. Rev. B **50**, 18 580 (1994).
[8] M. Ueda, O. Kitakami, Y. Shimada, Y. Goto, and M. Yamamoto, Jpn. J. Appl. Phys., Part 1 **33**, 6173 (1994).
[9] H. E. Fischer, H. Fischer, O. Durand, O. Pellegrino, S. Andrieu, M. Piecuch, S. Lefebvre, and M. Bessière, Nucl. Instrum. Methods Phys. Res. B **97**, 402 (1995).
[10] E. E. Fullerton, Y. K. Schuller, H. Vanderstraeten, and Y. Bruynseraede, Phys. Rev. B **45**, 9292 (1992).
[11] M. De Santis, A. de Andrés, D. Raoux, M. Maurer, M. F. Ravet, and M. Piecuch, Phys. Rev. B **46**, 15 465 (1992).
[12] E. Chason and T. Mayer, Crit. Rev. Solid State Mater. Sci. **22**, 1 (1997).
[13] K. Sinha, E. B. Sirota, S. Garoff, and H. B. Stanley, Phys. Rev. B **38**, 2297 (1988).
[14] V. Holý and T. Baumbach, Phys. Rev. B **49**, 10 668 (1994).
[15] V. Holý, J. Kubéna, I. Ohlídal, K. Lischka, and W. Plotz, Phys. Rev. B **47**, 15 896 (1993).
[16] P. Schlomka, M. Tolan, L. Schwalowsky, O. H. Seeck, J. Stettner, and W. Press, Phys. Rev. B **51**, 2311 (1995).
[17] F. Bridou and B. Pardo, J. Phys. III **4**, 1523 (1994).
[18] M. Li, M. O. Möller, and G. Landwehr, J. Appl. Phys. **80**, 2788 (1996).
[19] B. Vidal and P. Vincent, Appl. Opt. **23**, 1794 (1984).
[20] J. R. Lu, E. M. Lee, and R. K. Thomas, Acta Crystallogr., Sect. A: Found. Crystallogr. **52**, 11 (1996).
[21] L. G. Parratt, Phys. Rev. **95**, 359 (1954).
[22] E. Elkaim, S. Lefebvre, R. Kahn, J. F. Berar, M. Lemonnier, and M. Bessière, Rev. Sci. Instrum. **63**, 988 (1992).
[23] M. Bordessoule, S. Lefebvre, and M. Bessière (unpublished).
[24] Y. Yoneda, Phys. Rev. **131**, 2010 (1963).
[25] B. B. Mandelbrot, *The Fractal Geometry of Nature* (Freeman, New York, 1982).
[26] H. E. Fischer, H. Fischer, and M. Piecuch (in preparation).
[27] J. Daillant and O. Bélorgey, J. Chem. Phys. **97**, 5824 (1992).
[28] *Sasaki Tables* (National Laboratory for High Energy Physics, Japan).
[29] *CRC Handbook of Chemistry and Physics*, edited by D. R. Lide (CRC, London, 1994).
[30] A. de Bernabé, M. J. Capitán, H. E. Fischer, S. Lequien, C. Prieto, J. Colino, F. Mompeán, S. Lefebvre, M. Bessiere, C. Quirós, and J. M. Sanz, Vacuum (in press).